



## RESEARCH ARTICLE

# Characterization and computational simulation of human Syx, a RhoGEF implicated in glioblastoma

Ryan J. Boyd<sup>1</sup>  | Tien L. Olson<sup>1</sup> | James D. Zook<sup>1</sup> | Derek Stein<sup>1</sup> | Manuel Aceves<sup>1</sup> | Wan-Hsin Lin<sup>2</sup> | Felicia M. Craciunescu<sup>1</sup> | Debra T. Hansen<sup>1,3</sup> | Panos Z. Anastasiadis<sup>2</sup> | Abhishek Singharoy<sup>1</sup> | Petra Fromme<sup>1</sup> 

<sup>1</sup>Biodesign Center for Applied Structural Discovery, Arizona State University, Tempe, Arizona, USA

<sup>2</sup>Department of Cancer Biology, Mayo Clinic, Jacksonville, Florida, USA

<sup>3</sup>Center for Innovations in Medicine, Arizona State University, Tempe, Arizona, USA

## Correspondence

Ryan J. Boyd and Petra Fromme, Biodesign Center for Applied Structural Discovery, Arizona State University, 797 E Tyler Street, Tempe, AZ 85287, USA. Email: [rjboyd1@asu.edu](mailto:rjboyd1@asu.edu) and [Petra.Fromme@asu.edu](mailto:Petra.Fromme@asu.edu)

## Funding information

HHS | National Institutes of Health (NIH), Grant/Award Number: R01NS101721-A1; Mayo Clinic | Center for Clinical and Translational Science, Mayo Clinic (CCaTS); ASU | Biodesign Institute, Arizona State University

## Abstract

Structural discovery of guanine nucleotide exchange factor (GEF) protein complexes is likely to become increasingly relevant with the development of new therapeutics targeting small GTPases and development of new classes of small molecules that inhibit protein-protein interactions. Syx (also known as PLEKHG5 in humans) is a RhoA GEF implicated in the pathology of glioblastoma (GBM). Here we investigated protein expression and purification of ten different human Syx constructs and performed biophysical characterizations and computational studies that provide insights into why expression of this protein was previously intractable. We show that human Syx can be expressed and isolated and Syx is folded as observed by circular dichroism (CD) spectroscopy and actively binds to RhoA as determined by co-elution during size exclusion chromatography (SEC). This characterization may provide critical insights into the expression and purification of other recalcitrant members of the large class of oncogenic—Diffuse B-cell lymphoma (Dbl) homology GEF proteins. In addition, we performed detailed homology modeling and molecular dynamics simulations on the surface of a physiologically realistic membrane. These simulations reveal novel insights into GEF activity and allosteric modulation by the plekstrin homology (PH) domain. These newly revealed interactions between the GEF PH domain and the membrane embedded region of RhoA support previously unexplained experimental findings regarding the allosteric effects of the PH domain from numerous activity studies of Dbl homology GEF proteins. This work establishes new hypotheses for structural interactivity and allosteric signal modulation in Dbl homology RhoGEFs.

**Abbreviations:** CD, circular dichroism; DH, dbl homology; GBM, glioblastoma; GEF, guanine exchange factor; GEF720, alternate name for PLEKHG5; IMAC, ion metal affinity chromatography; PH, plekstrin homology; PI(4,5)P<sub>2</sub>, phosphatidylinositol 4,5-bisphosphate or PtdIns[4,5]P<sub>2</sub>; PIP, phospho-inositide phosphate; PLEKHG5, pleckstrin homology and RhoGEF domain containing G5; POPC, 1-palmitoyl-2-oleoyl-sn-glycero-3-phosphocholine; PPIs, protein-protein interactions; RhoA, RAS homology ortholog A; SEC, size exclusion chromatography; Syx, Synectin associated RhoGEF, alternate name for PLEKHG5.

This is an open access article under the terms of the [Creative Commons Attribution-NonCommercial-NoDerivs](https://creativecommons.org/licenses/by-nc-nd/4.0/) License, which permits use and distribution in any medium, provided the original work is properly cited, the use is non-commercial and no modifications or adaptations are made.

© 2022 The Authors. *The FASEB Journal* published by Wiley Periodicals LLC on behalf of Federation of American Societies for Experimental Biology.

**KEYWORDS**

Dbl homology, DH domain, GEF, glioblastoma, lipid binding protein, membrane-associated protein, molecular dynamics, oncogene, PH domain, PIP, protein dynamics, protein engineering, protein-protein interactions, RhoA, RhoGEF, small GTPase, structure-guided drug design

## 1 | INTRODUCTION

Recent successes designing drugs to inhibit small GTPase based drivers of oncogenesis and advances in modulating protein-protein interactions with structurally guided drug design have inspired renewed interest in characterizing the prolific family of small GTPase activating guanine exchange factor (GEF) proteins with the hope of establishing a new class of drug targets against this expansive class of potential oncogenes.<sup>1</sup> These proteins are responsible for modulating a diverse array of cell processes. Diffuse B-cell lymphoma (Dbl) family GEFs are the largest family of GEFs, containing 71-members out of 82 total RhoGEFs in humans.<sup>2</sup> Dbl GEFs facilitate the activation of small GTPases. The mechanistic details of GEF interaction with small GTPases have been reviewed previously.<sup>3</sup> The tightly controlled activation and localization of the small GTPase RhoA is directly coupled to stress fiber formation, cell mobility, and proliferation pathways via the opposing effects of Rho Activated Kinase (ROCK) and Diaphanous Homologue (Dia).<sup>4</sup> There is a three-fold higher prevalence of Rho activating GEFs (RhoGEFs) as compared to Rho GTPases (22 members in mammals) indicating that the GEFs are likely regulators of activation specificity for these pathways.<sup>5</sup> This is further corroborated by the fact that almost all GEF proteins have been shown to be tightly modulated by numerous mechanisms of inhibition or autoinhibition, suggesting that multiple layers of regulation acting on the GEF are needed for correct conditional flow of these signals within the cell.<sup>6,7</sup> Aberrant activation of these signals can be oncogenic; therefore, inhibitors to RhoGEF proteins could be potential cancer therapeutics.

Dbl family RhoGEFs are defined by two tandem domains—the DH-PH domains.<sup>8</sup> The 170–190 amino acid DH (Dbl homology) domain facilitates the exchange of guanine nucleotide bound within the small GTPase by structurally manipulating two “finger regions” that encapsulate the nucleotide binding pocket. Simultaneously, many GEFs also affect GDP binding with RhoA by moving a magnesium ion held in complex with Thr-37 and Thr-19 of RhoA out of its binding conformation with the phosphate groups of the RhoA-bound GDP<sup>5</sup> thereby reducing binding interactions. The approximately 120 amino acid pleckstrin homology (PH) domain is often responsible for binding phospho-inositide phosphate (PIP) lipid head

groups at the inner leaflet of the cell membrane.<sup>9,10</sup> In some cases, the PH domain allosterically activates the GEF activity of the protein or relieves autoinhibition<sup>11–13</sup> 0.2. While the mechanism and overall contribution of PH domain allostery are a matter of continuing study and vary in a protein dependent manner, it is quite clear that in general, GEFs are closely regulated in the cell and often have auto-inhibitory domains or are bound by other proteins to repress their activities when and where they are not intended to be active.<sup>14,15</sup> This spatiotemporal control keeps GEFs from spuriously activating their corresponding small GTPases.<sup>16</sup>

It is well established that spurious GEF activity and small GTPase activation are drivers of cell migration, cell proliferation and cancer progression.<sup>17,18</sup> Dachsel et al and others revealed that Syx is highly expressed in human glioma cells.<sup>19,20</sup> Experimental depletion of Syx in either glioma or endothelial cells disrupts cell polarity and suppresses response to chemotactic cues, thus inhibiting directed cell migration.<sup>19,21</sup> Notably, the inability of Syx depleted cells to migrate was rescued by the expression of exogenous Syx, but not by a Syx mutant with no GEF activity.<sup>19</sup> Additionally, depletion of Syx in conventional or patient-derived GBM cell lines inhibits GBM cell growth (unpublished observations). These results suggest that inhibition of Syx activity may be a possible treatment modality for GBM, and therefore, Syx warrants biophysical and structural characterization to facilitate structurally guided drug design.<sup>22,23</sup> Several structures of Dbl homology RhoGEF DH-PH domains have been solved previously, and GEF characterization methods have been established. In contrast, Syx is in a subgroup of Dbl homology GEFs that are largely uncharacterized outside of basic protein-protein interaction data<sup>24</sup> and no structural information is yet available for this protein.<sup>2</sup> Structural elucidation and drug screening efforts require production and purification of milligram quantities of monomeric protein. Failure to overcome protein expression and purification issues are the most common pitfall of structural characterization projects.<sup>25</sup>

Here we report the first high yield expression, and biophysical characterization of purified human RhoGEF Syx including characterization of RhoA binding activity of the Syx DH-PH domain, as well as computational analysis to support ongoing structural studies and drug design efforts.

## 2 | MATERIALS AND METHODS

### 2.1 | Sequence analysis and homology modeling

The full length Syx sequence (UniProt identifier: O94827-1, NCBI reference number: NM\_020631.6) was analyzed with the iTASSER homology-modeling server (Figure S1)<sup>26</sup> as well as PSIPRED,<sup>27</sup> SERP,<sup>28</sup> and XtalPred<sup>29</sup> servers. The resultant disorder prediction and structural information were used to guide where truncation would be most appropriate. Several truncation sequences were made based on designing constructs that contained the DH and PH domains but removed unordered regions that would interfere with structural studies. The patterns of truncations were also guided by sequence alignments with Rho GEF structures 1XCG, 1X86, and 3ODO (PDZRhoGEF, LARG, and P115-RhoGEF respectively). Sequences were aligned with the MAFFT server using the L-INS-i method.<sup>30</sup>

### 2.2 | Model building and molecular dynamics

Known RhoGEF-RhoA complex structures (1XCG, 1X86, 2RGN, 4XH9, 4DON) were structurally aligned with the Syx homology model to produce an initial Syx-RhoA model. This model was then repeatedly refined using Rosetta docking protocols.<sup>31,32</sup> The resulting homology model of Syx was structurally aligned with several other known structures of PH domains and visually compared to structures containing bound lipid head groups to estimate the orientation of a potential lipid binding pocket on Syx.<sup>9,33-35</sup> The Bio Chemical Library (BCL) software package was used to generate lipid headgroup conformers and Rosetta ligand docking protocols were used to place a PI(4,5)P<sub>2</sub> lipid into the putative binding pocket.<sup>36,37</sup> The Orientations of Proteins in Membranes (OPM) server and CHARMM-GUI membrane builder were used to add a geranylgeranyl group to the tail of RhoA and then generate an all atom simulated membrane bilayer around the OPM generated lipid-protein interface, as well as place waters and NaCl ions throughout the box.<sup>38-40</sup> Parameter files for GDP, GTP, magnesium, POCP, PI(4,5)P<sub>2</sub>, and geranylgeranyl groups were either generated by CGenFF or found in CHARMM36m params files. NAMD 2.14-CUDA utilizing the CHARMM36m force field was used to run a NPT simulations with 2 fs timesteps for approximately 1.2  $\mu$ s after equilibration.<sup>41-43</sup> A temperature of 300°K and 1 atm of pressure was maintained by a Langevin thermostat and barostat and electrostatics were calculated with the particle mesh Ewald method. All simulations were run on GTX1080 Nvidia GPUs until RMSD values reached

equilibrium and visual observation confirmed that lipids were correctly oriented.<sup>44</sup>

### 2.3 | Dynamic network analysis

Dynamic network analysis was performed as described in Sethi et al.<sup>45</sup> Nodes were defined as C $\alpha$  carbons, or phosphates. Community analysis of groups of residues that are most strongly interconnected was performed using the Girvan-Newman algorithm and visualized with VMD. Optimal path analysis was performed between several residues that clearly bind membrane lipids on both the PH and DH domain of Syx protein and residue Thr-37, located at the center of switch I region of RhoA.

### 2.4 | Protein engineering and mutagenesis

CamSol analysis was performed by uploading the Syx homology model and sequence to the CamSol server.<sup>46</sup> The resulting prediction was encoded into the B-factor of the protein and visualized with PyMol. Mutants at these sites were either picked by hand or because they were scored favorably by the Rosetta design protocol.<sup>47</sup>

### 2.5 | Expression optimization

Initial expression constructs containing several truncated versions of wild-type mouse Syx homologs were generated by the Anastasiadis lab. Chemo-competent BL21(DE3) cells (New England Biolabs) were transformed according to the manufacturer's instructions. A single resultant colony was isolated and then used to inoculate a 5 ml liquid culture containing TB containing 12 g/L tryptone, 24 g/L yeast extract, 4 ml/L glycerol, 2.31 g/L KH<sub>2</sub>PO<sub>4</sub> (17 mM), 12.54 g/L K<sub>2</sub>HPO<sub>4</sub> (72 mM), with appropriate antibiotic.<sup>48</sup> Cell stocks were made by adding glycerol to 30% and stored at -80°C.

Starter cultures were inoculated by using a sterile pipette tip to transfer a small chunk of frozen glycerol stock into 1 ml of pre-warmed TB. After overnight growth, this starter culture was visually checked for cell growth (with a desired OD<sub>600</sub> of approximately 0.8) and added to an autoclaved 250 ml baffled flask containing 50 ml of Terrific Broth (TB) and cells were allowed to grow at 37°C. IPTG was added to a final concentration of 0.5 mM when the culture reached an OD<sub>600</sub> of 0.8, and 1 ml aliquots were taken for analysis at desired time points. For subsequent SDS-PAGE analysis, aliquots were centrifuged at 17K $\times$  g and the supernatant was discarded. 10  $\mu$ l of cell pellet

was mixed with 500  $\mu$ l 1X Laemmli buffer (Bio-Rad Cat# 1610747) and stored at  $-20^{\circ}\text{C}$ . Samples were incubated at  $95^{\circ}\text{C}$  for 5 min and spun down at  $17\text{K} \times g$  for 10 min to remove cell debris before analysis of raw supernatant was performed via SDS-PAGE using a 12% acrylamide-tris gel and subsequent overnight transfer to a Western blot PVDF membrane and visualization with an anti-His antibody (Figure 1) (Qiagen Cat# 34440, RRID:AB\_2714179).

Further optimization was done with His6-TEV-SyX<sub>393-792</sub>. This construct was transformed into BL21(DE3) (NEB), BL21(PlysS)(NEB), Lemo21(DE3) (NEB), BL21-AI(Invitrogen), KTD101(DE3), KJ740(DE3), C41(DE3), and C43(DE3) strains of *Escherichia coli* cells. Strain KJ740 was obtained from the Yale *E. coli* Genetic Stock Center (CGSC), and the (DE3) lysogen was made using the  $\lambda$ DE3 Lysogenization Kit 538 (EMD Millipore #69734-3). Expression was performed as described above apart from chloramphenicol being used with Lemo strains. Trials with 1 and 2 mM of Rhamnose were tested with the Lemo21(DE3) cells. For BL21-AI, arabinose at 0.2% final concentration was added along with IPTG at induction, and TB medium contained 0.1% glucose.

## 2.6 | Cloning

Codon optimized constructs of the truncated versions of human Syx were designed and obtained from GenScript. Fusion constructs were generated as described previously<sup>48</sup>

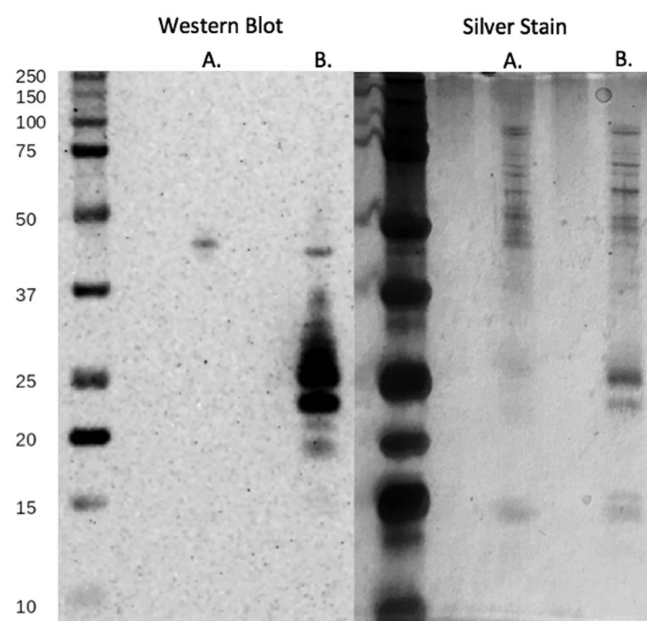


**FIGURE 1** Comparison of expression of mouse Syx<sub>406-799</sub> and codon optimized human Syx<sub>393-792</sub> genes. Identical fractions were visualized with silver stain and western blot (lanes A. Human Syx<sub>393-792</sub>; MW 48.3 kDa. Lanes B. Mouse Syx<sub>406-799</sub>; MW 46.6 kD).

by cloning our codon optimized Syx gene into parent vectors containing the following tags that are cleavable with tobacco etch virus (TEV) protease: N-terminal His6 plus maltose binding protein (MBP; RRID:Addgene\_29708); C-terminal MBP plus His6 (Addgene\_37237); N-terminal His6 plus glutathione S-transferase (GST; RRID:Addgene\_29707); N-terminal His6 plus small ubiquitin-like modifier (SUMO; RRID:Addgene\_29711); or N-terminal His6 plus green fluorescent protein (GFP; RRID:Addgene\_29716). Note that in the plasmid names for this clone the numbering of Syx residues was based on the Syx isoform from NCBI Reference Sequence NP\_001036128.1. The sequence of this isoform is identical to the UniProt sequence O94827-1 used for the computational studies, aside from an additional 56 amino acids at the N-terminus of NP\_001036128.1. All constructs were transformed into both BL21(DE3) and T7 Express lysY/Iq high competency *E. coli* (New England Biolabs #C30131). Ligation independent cloning was performed with the In-Fusion HD Cloning Plus system (Clontech #638910). Plasmid DNA was prepared with the QIAprep Spin Miniprep (QIAGEN #27106). DNA sequences were verified by Sanger sequencing at the DNA Laboratory core facility at Arizona State University or at GenScript.

## 2.7 | Preparation scale *E. coli* expression

A 5 ml overnight growth of the N-terminal His6-MBP-TEV-SyX<sub>393-792</sub> (referred to as MBP-SyX<sub>393-792</sub> for brevity, or SyX<sub>393-792</sub> if referring to protein which has undergone TEV cleavage and MBP removal) construct in T7 Express lysY/I<sup>q</sup> *E. coli* was visually checked for cell growth (OD<sub>600</sub> of approximately 0.8) before being added to 1 L of pre-warmed TB containing 100  $\mu\text{g}/\text{ml}$  ampicillin. Cells were grown at  $37^{\circ}\text{C}$  and 300 rpm shaking to an OD<sub>600</sub> of 0.8. The temperature was decreased to  $25^{\circ}\text{C}$  and IPTG was added to a final concentration of 0.4 mM. Cells were allowed to grow for another 4 h before being spun down. Cell pellets were weighed and resuspended in 10 ml Lysis Buffer A per 1 g of cells, and the resulting slurry was frozen at  $-80^{\circ}\text{C}$ . Lysis Buffer A contained PBS (137 mM NaCl, 2.7 mM KCl, 10 mM Na<sub>2</sub>PO<sub>4</sub>, 1.8 mM KH<sub>2</sub>PO<sub>4</sub>, pH 8), 2 mM dithiothreitol (DTT), protein inhibitor cocktail (Roche cComplete Ultra, Sigma part no. 5892791001), 1 mM PMSF.

## 2.8 | Purification of *E. coli* derived MBP-SyX<sub>393-792</sub>

Frozen cells were resuspended in  $4^{\circ}\text{C}$  lysis buffer and 2 mg/ml hen egg lysozyme (Sigma part no. 4403) and 0.2 mg/ml bovine pancreas DNase (Sigma part no.



9003-98-9) were added. The thawing cell slurry was sonicated on ice at 50% power for 1 s on, 2 s off, for 1 min using a Branson 550 sonicator. The resulting slurry was centrifuged at 40 000 g for 15 min at 4°C and then filtered through a 0.45  $\mu\text{M}$  filter before using a 150 ml superloop connected to an AKTA FPLC in a 4°C cold room to load protein at 0.5 ml/min onto a 5 ml amylose column (Cytiva Product no. 28918779). The column was previously equilibrated with buffer A (10 mM  $\text{Na}_2\text{PO}_4$ , 1.8 mM  $\text{KH}_2\text{PO}_4$ , pH 8, and 1 mM TCEP). The protein was washed with 10 column volumes at 5 ml/min and then eluted in 1 ml fractions with buffer A plus 50 mM maltose. Fractions with an absorbance peak at 280 nm (combined volume of 20–25 ml at a protein concentration of 1–5 mg/ml) were concentrated to a volume of 500  $\mu\text{l}$  using a 30 kD Molecular Weight Cut Off (MWCO) spin concentrator (Millipore part no. UFC903096) spun at 3000 g, while visually ensuring there was no turbidity and mixing the solution every 5 min with a pipette. The concentrated sample was injected onto a pre-equilibrated Superdex 200 Increase 30/100 GL column (Cytiva part no. 28990944) and run at 0.4 ml/min at 4°C with buffer A. Peaks were pooled and stored at 4°C. The protein concentration and yield was determined at this stage by absorbance at 280 nm ( $A_{280}$ ), using a molar extinction coefficient of 112 355  $\text{M}^{-1} \text{cm}^{-1}$  for the MBP-Syx<sub>393–792</sub> fusion construct. SDS-PAGE gels were run on all fractions and stained with Coomassie to ascertain purity.

## 2.9 | TEV cleavage and negative purification

The fractions containing purified protein at the expected molecular weight as determined by Coomassie stained SDS-PAGE gel were cleaved with TEV protease by incubating a 10:1 ratio of protein and TEV mixture overnight at 4°C in buffer A. This mix was then incubated with 3 ml of nickel NTA slurry for 20 min to remove the His tagged MBP and TEV. Flow-through and subsequent washes were collected and concentrated using a 30 kDa Molecular Weight Cut Off (MWCO) spin concentrator (Millipore part no. UFC903096). Protein concentrations were confirmed with  $A_{280}$  measurements after each interval with a molar extinction coefficient of 39880  $\text{M}^{-1} \text{cm}^{-1}$  for the cleaved Syx<sub>393–792</sub>. Presence of the correct protein species was confirmed routinely with western blot. RhoA (1 mg/ml) and anti-Syx antibody were blotted directly on PVDF as control before blocking with BSA (Figure S8). Anti-Syx antibody (Proteintech Cat# 19830-1-AP, RRID:AB\_10858324) (8  $\mu\text{l}$  in 10 ml of TBST) was used in conjunction with a goat anti-rabbit

antibody (Jackson ImmunoResearch cat# 111-035-003, RRID: AB\_2313567) for visualization.

## 2.10 | Size exclusion chromatography

The superdex 200 column was connected to the AKTA FPLC in the 4°C cold room and equilibrated with at least 2 column volumes of sterile filtered water followed by at least 2 column volumes of 25 mM HEPES, 150 mM NaCl, and 1 mM TCEP buffer until the  $A_{280}$  and conductance traces appeared constant. Samples were spun down at 17 000 g for 10 min in a tabletop centrifuge at 4°C before 500  $\mu\text{l}$  of sample was injected onto the column and run at 0.4 ml/min for the entire run. Fractions were collected at 1.5 ml intervals over 1.5 column volumes. After each run, the column was re-equilibrated for 2 column volumes before the next run was initiated. A standard curve was run periodically to determine the elution volume which corresponded to the molecular radius of each protein (Cytiva part no. 28403842). Peaks eluting before 8 ml were considered to be in the void volume of this column.

## 2.11 | Dynamic light scattering

The monodispersity of the purified protein was ascertained with a Molecular Dimensions SpectroSize 302 DLS apparatus with a 785 nm 60 mW laser imaging of 2  $\mu\text{l}$  protein droplets suspended in a 24 well hanging drop plate. The DLS data were collected in 10 scans with 20 min long scans each, and resultant data was examined by the cumulants method<sup>113</sup>. DLS based buffer screening was done by mixing 2  $\mu\text{l}$  of protein with 2  $\mu\text{l}$  of each well of the Hampton research buffer screen 1 and 2 kits (CAT NO: HR2-072, HR2-413) and incubated for 1 h before testing with DLS.

## 2.12 | RhoA expression and purification

RhoA plasmid (RRID:Addgene\_73231) expressing the TEV cleavable N-terminal His6-tagged soluble domain of RhoA including residues 1–184 (referred to as His6-TEV-RhoA<sub>1–184</sub> or just RhoA unless otherwise stated) was transformed into Rosetta 2 BL21(DE3) cells and frozen as glycerol stocks that were used to inoculate 5 ml overnight starter cultures grown overnight at 37°C, 250 rpm. 5 ml overnight starter cultures were used to inoculate 2 L baffled flasks containing 1L of TB media with antibiotic and allowed to grow at 37°C until the culture reached an OD<sub>600</sub> of 0.6–0.8. At this point, 250 mM of IPTG was added, the temperature was turned down to 18°C, and the culture was allowed to grow overnight. The

**TABLE 1** Secondary structure prediction by various methods. Back calculated secondary structure prediction of homologous GEF crystal structures generated by PDB2CD are shaded in grey, including a Syx homology model

Method	Helix	B-sheet	Turns	Unordered	NRMSD	Homology
BeStSel	30.1%	24.6%	8.6%	36.7%	0.013	
CDSSTR (SMP180)	54.0%	10.0%	10.0%	24.0%	0.014	
K2D3	36.2%	20.1%		43.8%		
Syx model	47.2%	10.9%				100%
(PDZRhoGEF) 1XCG	47.1%	16.7%				25.8%
(P115-RhoGEF) 3ODW	57.7%	14.0%				23.9%
(LARG-RhoGEF) 1X86	48.7%	13.0%				21.4%

resulting culture was spun down at 4000 rpm, and the pellet was weighed and frozen at  $-80^{\circ}\text{C}$ .

### 2.13 | RhoA purification

Critically, all buffers were supplemented with  $50\ \mu\text{M}$  GDP (Sigma cat no. G7127) to maintain RhoA in a folded state. Seven grams of cells were homogenized with 80 ml of Lysis Buffer (Tris-HCl pH 8.0, 150 mM NaCl, 2 mM  $\text{MgCl}_2$ , 50  $\mu\text{M}$  GDP, 10% glycerol, 5 mM imidazole, 1 mM PMSF, 1 SIGMAFAST ETDA-free protease inhibitor cocktail tab (Sigma sku S8830-20TAB), 2 mg/ml lysozyme, 2 mM TCEP). Cells were lysed via probe-sonication with a Branson 550 sonicator set to run in intervals of 1 s on, 2 s off for a total of 1 min at 50% power. Sonication was repeated two times before the lysate was spun down at 40 000 rcf for 20 min at  $4^{\circ}\text{C}$ . The resulting supernatant was passed through a  $0.45\ \mu\text{m}$  syringe filter before the supernatant was added to a 150 ml superloop attached to a GE Akta series FPLC running unicorn 7 software to automate the following protocol: The clarified supernatant was injected at 1 ml/min onto a 5 ml Ni-NTA column (Cytiva part no. 17524802) equilibrated with Wash Buffer (50 mM Tris-HCl pH 8.0, 500 mM NaCl, 2 mM  $\text{MgCl}_2$ , 50  $\mu\text{M}$  GDP, 10% glycerol, 15 mM imidazole, 2 mM TCEP). The column was washed at 5 ml/min with 10 column volumes of wash buffer before a linear gradient of Elution buffer (50 mM Tris-HCl pH 8.0, 300 mM NaCl, 2 mM  $\text{MgCl}_2$ , 50  $\mu\text{M}$  GDP, 10% Glycerol, 200 mM Imidazole, 2 mM TCEP) was used to elute the bound protein.<sup>49</sup> Fractions of the elution step were collected and run on an SDS-PAGE gel before being stained with Coomassie to reveal fractions containing bands corresponding to the molecular weight of RhoA at 22 kDa. Fractions were pooled, and an  $A_{280}$  absorbance trace was measured using the elution buffer as a blank to estimate protein concentration and overall yield. The presence of His6-TEV-RhoA<sub>1-184</sub> was also confirmed with Western blot using an anti-RhoA antibody (Thermo Fisher Scientific Cat# MA1-134, [RRID:AB\\_2536840](https://pubmed.ncbi.nlm.nih.gov/2536840/)).

### 2.14 | RhoA-MBP-SyX<sub>393-792</sub> complex formation

Several methods for complex formation were tested to assess the most effective protocol for forming the MBP-SyX<sub>393-792</sub>-RhoA complex to ascertain which produced the highest quality protein. The following protocols used Un-cleaved MBP-SyX<sub>393-792</sub> (unless otherwise stated) incubated at  $4^{\circ}\text{C}$  with un-cleaved His6-TEV-RhoA<sub>1-184</sub> in a 1:2 ratio for 1 h in all five trials. In “mix 1” (Figure 3A, purple trace), 10 mM of EDTA was added to the mixture to chelate magnesium out of the GDP binding site of RhoA. “mix 2” (Figure 3A, red trace) used cleaved SyX<sub>393-792</sub> (Figure 3B) mixed with RhoA, and also contained 10 mM EDTA to chelate magnesium. “mix 3” (Figure 3A, black trace) contained MBP-SyX<sub>393-792</sub> mixed with RhoA which was buffer exchanged 6 times in a 10k MWCO spin concentrator to remove all buffer containing GDP. In “mix 4” (Figure 3A, light blue trace) an excess of ammonium sulfate was used to precipitate a protein mixture containing both MBP-SyX<sub>393-792</sub> and RhoA in order to competitively force GDP out of the active site of RhoA and remove GDP containing buffer. For “mix 5” (Figure 3A, grey trace) the process was the same as “mix 4” except that the ammonium sulfate precipitation was performed on RhoA alone, then MBP-SyX<sub>393-792</sub> protein solution was added to the RhoA. Each resulting solution was run on a Superdex 200 column as previously described. Controls show RhoA (Figure 3A, green trace), MBP-SyX<sub>393-792</sub> (Figure 3A, orange trace), and a molecular weight control (Figure 3A, dark blue trace).

### 2.15 | Circular dichroism

Cleaved SyX<sub>393-792</sub> was buffer exchanged four times into CD buffer (150 mM sodium fluoride adjusted to pH 7.5 with 50 mM monobasic and dibasic sodium phosphate) using a 15 kDa MWCO Amicon spin column. The circular dichroism (CD) spectra were measured on a Jasco

J-815 circular dichroism spectrophotometer scanning from 190–260 nm.<sup>50</sup> The resulting spectra were analyzed by the servers BeStSel, K3D2, and DichroWeb's CDSSTR protocol using the SMP180 basis set.<sup>51–53</sup> Spectral analysis was compared to CD spectra of homology models and known protein structures with homology greater than 20% (Table 1, column 7 labeled “Homology”) by back-calculating CD spectra with the PDB2CD server to check that the experiment accurately recapitulated secondary structure of the predicted folds seen in the homology model.<sup>54</sup>

### 3 | RESULTS

#### 3.1 | Sequence analyses & homology modeling guided construct optimization for structural studies

To assess which regions of Syx were most likely to be ordered and determine which domains were likely to be useful targets for structural discovery, a homology model and corresponding sequence analysis were performed. Sequence identity between Syx and the most homologous proteins that have solved structures indicated a sequence identity of approximately 25% (Figure S1). Homology modeling of Syx DH-PH fragments predictably produced a model largely similar to known homologous structures; however, regions of the DH and PH domain have several stretches that were unable to be modeled reliably as determined by their homology to known structures<sup>123</sup>. Most notably a loop on the PH domain had no matching homology anywhere in the PDB (Figure S1). Analyses of the full-length Syx protein using iTASSER<sup>55</sup> and DISOPRED3<sup>56</sup> showed that the regions flanking the DH and PH domain were predicted to contain intermittent regions of highly disordered loops and poly-glutamate stretches. These regions were predicted to be poor targets for structural discovery; therefore, truncation of the wild type protein was warranted.

#### 3.2 | Expression screens generate reliable protein production conditions

HIS-tagged mouse Syx constructs received from the Anastasiadis lab contained Syx GEF domains with truncations over four residue ranges: (1) 290–799, (2) 290–748, (3) 406–799, (4) 406–748, as well as a GST-tagged full-length mouse Syx. Expression in *E. coli* was only observable for mouse construct Syx<sub>406–799</sub>, which showed modest expression with several unwanted lower molecular weight bands for the mouse Syx protein (Figure 1, lane B). Screening

of expression conditions revealed that peak protein levels were achieved within 4 h of induction at 25°C. At this juncture, a human homologue of the Syx<sub>406–799</sub> mouse construct we refer to as Syx<sub>393–792</sub> was optimized for expression in *E. coli*. Screening showed meager enhancement of expression, but more importantly it showed none of the unwanted lower molecular weight bands seen in the mouse construct (Figure 1, lane A [human optimized] vs. lane B [mouse native]). Marginal improvements in yield were achieved by using T7 Express *lysY/I<sup>q</sup>* BL21(DE3) *E. coli* (NEB; Figure S2). We then aimed to further improve on the codon-optimized construct with the addition of various fusion proteins for enhanced solubility and purification (Figure S3). We also attempted small-scale IMAC (Ion Metal Affinity Chromatography) purification; however, we were not able to recover any substantial amount of protein. When expression was screened on several fusion constructs, the N-terminal MBP-Syx fusion construct produced large quantities of protein which were clearly visible on a Coomassie stained SDS-PAGE gel at the correct molecular weight (Figure S4).

#### 3.3 | Size exclusion chromatography & dynamic light scattering reveal pure, milligram quantities of MBP-Syx<sub>393–792</sub> with a high molecular radius

Protein quality after expression was tested via size exclusion chromatography (SEC) and DLS. Purification of the MBP-Syx<sub>393–792</sub> via amylose column and SEC was confirmed to be over 90% pure by Coomassie stained SDS-PAGE (Figure S4). Protein yields after amylose column were approximately 10 mg per liter of culture. DLS showed presence of an aggregate with a particle sized ~17 nm and a polydispersity index (PDI) of 0.54 indicating a mixture of populations (Figure S5). All SEC runs with MBP-Syx<sub>393–792</sub> on a Superdex-200 increase 30/100 GL SEC column resulted in a large clearly visible peak eluting at or near the void volume of the column, around 8 ml (Figure 2). This occurred regardless of changes in pH from pH 10 to pH 5, below which no protein was visible indicating that it had crashed out of solution. In addition to the conditions shown in Figure 2, trials of numerous common buffer additives commonly used to reduce aggregation including PBS, Tris, and HEPES (pH 7–8), 0–500 mM NaCl, 1–5 MgCl<sub>2</sub>, 2 mM MgSO<sub>4</sub>, 500 mM (NH<sub>4</sub>)<sub>2</sub>SO<sub>4</sub>, 0.1% Triton X-100, 0.1% Tween20, 0.1% Tween80, 0.1%–1% β-DDM, 0.1% β-OG, 0.1% CHAPS, 1–10 mM EDTA, 1–5 mM DTT, 1–5 mM β-ME, 1 mM TCEP, 10% ethanol, 5%–30% glycerol, 250 mM glucose, 500 mM Arginine L-HCL, 50 mM Arginine L-HCl + 50 mM L-glutamic acid were not effective.<sup>57</sup>

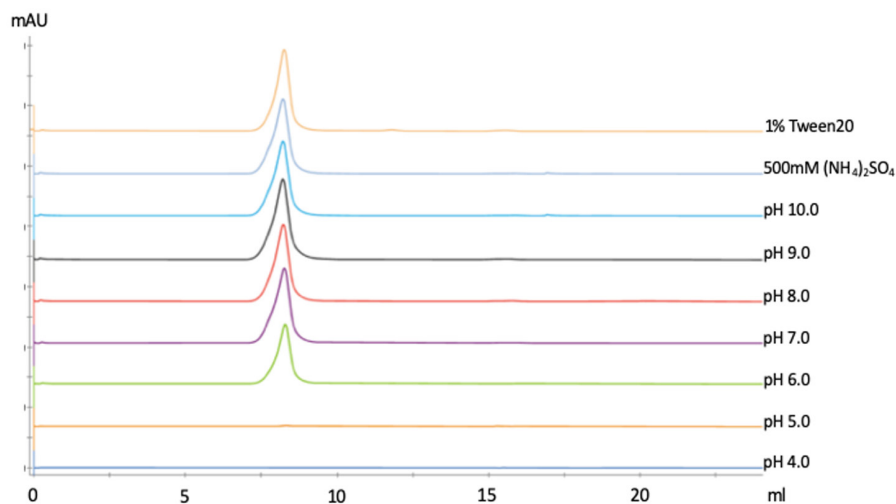


**FIGURE 2** Screening of SEC buffer conditions did not produce monomeric MBP-SyX<sub>393-792</sub> as shown by SEC absorbance trace at 280 nm. Each sample was from the same preparation of MBP-SyX<sub>393-792</sub> and differed only by the buffer additives indicated in the legend. Buffers all contained 500 mM NaCl, and also contained the following buffers: pH 4–5: 20 mM sodium acetate buffer, pH 6: 20 mM sodium citrate, pH 7: 20 mM sodium phosphate, pH 8: 20 mM Tris, pH 9: 20 mM glycine, and pH 10: 20 mM CAPS buffers. 1% Tween20 and 500 mM (NH<sub>4</sub>)<sub>2</sub>SO<sub>4</sub> respectively were both added to a base buffer of 20 mM HEPES pH 7.5, 500 mM NaCl in the case of the final two SEC runs.

These results are indicative of a soluble aggregate or very large homo-oligomer. The best conditions established (10 mM Na<sub>2</sub>PO<sub>4</sub>, 1.8 mM KH<sub>2</sub>PO<sub>4</sub>, pH 8) were able to generate a very small peak corresponding to monomeric protein (MBP-SyX<sub>393-792</sub> control shown in orange [Figure 3A](#)). When the peak corresponding to the molecular radius of monomeric protein was isolated and re-run on the same SEC column, the result was a similar equilibrium of two peaks with the predominant population in the void volume. Solubility screening using Hampton detergent and additive screens were not successful at reducing the presence of the aggregate as measured by DLS.

### 3.4 | RhoA–SyX<sub>393-792</sub> complex formation

Size exclusion chromatography was used to visualize peak shifts that indicate the formation of a protein-protein complex upon mixing MBP-SyX<sub>393-792</sub> or cleaved SyX<sub>393-792</sub> with RhoA (Protein domains shown in [Figure 3B](#), cleavage shown in [Figure 3C](#)). The SyX<sub>393-792</sub>-RhoA complex was formed in several different trials to establish conditions which would produce a monodisperse complex suitable for structural studies. RhoGEF DH-PH domains are expected to have the highest affinity for RhoA when it has no nucleotide bound; therefore, removal of GDP is likely necessary to drive complex formation with Syx. Most small GTPases are unstable in their apo form and quickly degrade without GDP or a GEF stabilizing them. This step was complicated by the high binding affinity of GDP with RhoA, which required optimization to find conditions

which do not drive aggregation but still effectively remove GDP.

The dashed line in each of the SEC traces in [Figure 3A](#) indicates absorbance at 260 nm which is the absorbance peak for nucleotides like GDP, while the solid line shows the absorbance at 280nm. Peaks where the 260 nm absorbance signal is greater than 280 nm absorbance signal suggest the presence of lingering GDP. This condition also shows the largest peak shifted towards lower retention times, suggesting the presence of a complex which was larger than the control trace of Syx alone ([Figure 3A](#), orange trace). This was confirmed by SDS-PAGE analysis showing bands at the correct molecular weights for SyX<sub>393-792</sub> and RhoA in this fraction ([Figure 3D](#)).

### 3.5 | CD spectroscopy indicates that *E. coli* expressed SyX<sub>393-792</sub> has characteristic spectra of a folded protein

CD spectroscopy was performed to ascertain if cleaved SyX<sub>393-792</sub> was folded correctly by comparing the experimentally predicted secondary structure with the secondary structure of known highly homologous crystal structures. Analysis of the CD spectra of Syx predicted an  $\alpha$ -helical content of 30%–56% and a  $\beta$ -sheet content of 10%–24% depending on the algorithm used. CD results were checked by feeding an iTASSER homology model into PDB2CD that resulted in a plausible secondary structure prediction of 47% helix and 10.9%  $\beta$ -sheet ([Table 1](#), row 4 labeled “Syx model”).<sup>58</sup> Therefore, CD indicates the presence of a



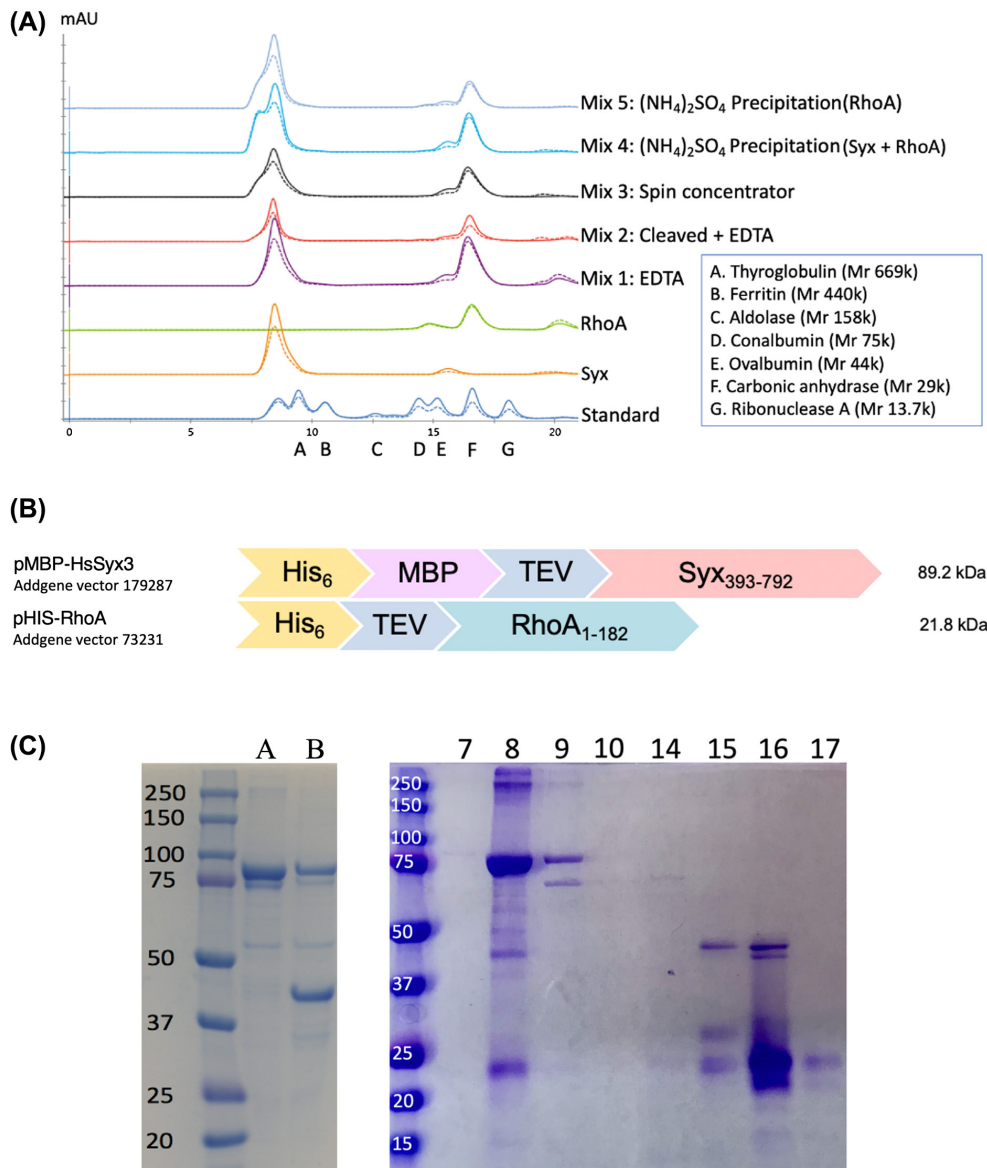


**FIGURE 3** (A) SEC absorbance trace at 280 nm of mixtures of MBP-Syx<sub>393-792</sub> and RhoA after using varying strategies for removing GDP from RhoA to induce the formation of a high affinity MBP-Syx<sub>393-792</sub>-RhoA complex. The composition of each SEC trace is as follows: Shown in purple, “Mix 1” contains MBP-Syx<sub>393-792</sub>-RhoA with 10 mM of EDTA to chelate magnesium out of the GDP binding site of RhoA; shown in red, “Mix 2” used cleaved Syx<sub>393-792</sub> mixed with RhoA, also with 10 mM EDTA; shown in black, “Mix 3” contained MBP-Syx<sub>393-792</sub> mixed with RhoA which was buffer exchanged six times in a 10k MWCO spin concentrator to remove GDP; shown in light blue, “mix 4” an excess of ammonium sulfate was used to precipitate a protein mixture containing both MBP-Syx<sub>393-792</sub> and RhoA to remove GDP; Shown as a grey trace “mix 5” the process was the same as “mix 4” except that the ammonium sulfate precipitation was performed on RhoA alone before being mixed with MBP-Syx<sub>393-792</sub>. All complex formation mixes were made as 1:1 mixtures and each combination was allowed to equilibrate for 1 h. The green trace labeled “RhoA” shows RhoA control and orange trace labeled “Syx” shows MBP-Syx<sub>393-792</sub> control. MW of N-term MBP-Syx is 90.8 kDa. RhoA is 22 kDa. The protein standard shown in dark blue and labeled as “standard” consists of A. Thyroglobulin (Mr 669 000), B. Ferritin (Mr 440 000), C. Aldolase (Mr 158 000), D. Conalbumin (Mr 75 000), E. Ovalbumin (Mr 44 000), F. Carbonic anhydrase (Mr 29 000), G. Ribonuclease A (Mr 13 700). (B) Cartoons depict expressed protein fusion constructs of both MBP-Syx<sub>393-792</sub> and RhoA. RhoA is truncated at residue 184 to remove its highly charged linker and geranylgeranyl transferase recognition site. (C) MBP-Syx<sub>393-792</sub> (lane A) cleavage with TEV protease produces an approximately 48 kDa band (lane B) corresponding to the molecular weight of Syx<sub>393-792</sub> (48 kDa and MBP 42 kDa), indicative of successful cleavage. (D) Coomassie Gel of fractions from SEC run “mix 4” shows the presence of bands corresponding to the correct molecular weight for RhoA and MBP-Syx<sub>393-792</sub>. Bands in fractions at 8 and 9 ml indicate the presence of MBP-Syx<sub>393-792</sub> and RhoA where bands in fraction 15, 16, and 17 ml indicate the presence of RhoA and cleaved MBP-Syx<sub>393-792</sub> due to background cleavage activity at the TEV site.

folded protein (Figure 4) with similar secondary structure characteristics as Syx homologues (Table 1, row 5, 6, 7).

### 3.6 | Biophysical surface analysis

The homology model of Syx was analyzed by several methods to ascertain why size exclusion results suggest the presence of an aggregated protein.

Homology models were analyzed with the protein-sol server that produced protein models scoring the ratio of solvent accessible non-polar residues to polar residues at a given location in the sequence to illustrate relative hydrophobicity of the structure. The analysis also calculated electrostatic potential of the protein surface using a Finite Difference Poisson-Boltzmann (FDPB) method to score the structure such that it can be visualized based on charge distribution (Figure S5).<sup>59</sup>

The analysis revealed a hydrophobic loop on the PH domain of Syx that is un-conserved among structures in the PDB database despite being fairly conserved in the NCBI sequence database (Figure S1). This loop may influence interaction with the membrane or drive interactions with other hydrophobic domains (Figure 5, indicated as a purple-black dashed box and corresponding dashed purple-black bracket). Visualization of charge distribution also showed that the protein was highly polar and had a predominantly positive charge all over the DH domain including the RhoA binding site,<sup>60</sup> and a highly negative charge on the PH domain, except for a few membrane facing loops (Figure S5).

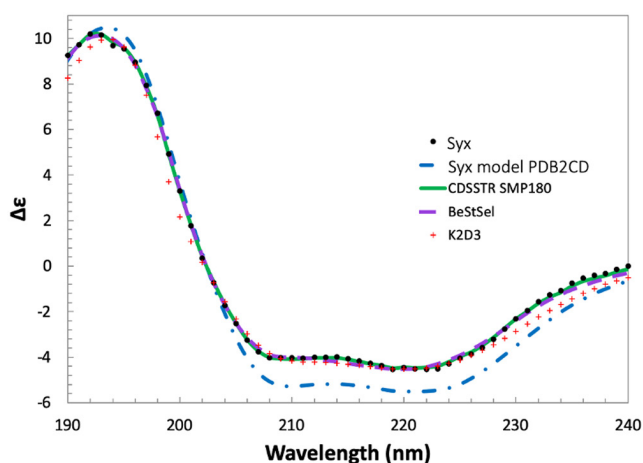


**FIGURE 4** CD spectral analysis of Syx. Experimental spectra is shown as black dots in the plot below. Fits of CDSSTR (SMP180), BeStSel, and K2D3 CD analysis algorithms are shown as purple dashes, green line and red + respectively. The predicted spectra of Syx based on the homology model is shown in blue dashes.

### 3.7 | Protein engineering

Structurally corrected CamSol web server<sup>46</sup> predictions indicated that several arginine residues were potentially driving aggregation, shown as redder areas on the cartoon (Figure 6). These predictions coincided with several predictions made by Rosetta design for stabilizing mutations. After manual curation of predicted sites, positions R466, R562, and R698 (Figure 6 cartoon) were chosen for site directed mutagenesis. Protein was purified and analyzed identically to Figure 3 MBP-Syx<sub>393–792</sub> control (orange trace). SEC of mutants revealed several shifts towards higher retention on the column suggesting a reduction in molecular radius of the aggregate (Figure 6 blue, orange, and green trace).

### 3.8 | Molecular dynamics simulations recapitulate interactions seen in RhoGEF crystal structures and suggest mechanisms of membrane allostery

An all atom molecular dynamics simulation of the full length Syx-RhoA complex (Figure 7A, cropped for visualization) was performed to observe if the protein-lipid interface between Syx and the membrane produced significant structural reorganization of hydrophobic loops, and dynamic network analysis was performed to attempt to detect interactions that might produce allosteric effects on the active site of RhoA.

Dynamic network analysis revealed that these simulations accurately recapitulated binding interactions that have been observed in other co-crystal structures of Dbp family RhoGEFs with RhoA (Figure 7B).<sup>3,61</sup> Both the “switch I” and “switch II” region of RhoA were shown to interact with the DH domain of Syx (Figure 7B).<sup>62</sup> Syx interactions with the “switch I” region of RhoA were observed to co-vary with several residues responsible for binding the magnesium co-factor that interacts with the di-phosphate moiety of GDP, including Thr-19, Thr-37, and Asp-59. Displacement of this magnesium is expected to be pivotal for hypothesized mechanisms of guanine exchange.<sup>63</sup>

Optimal path analysis to determine the most significant interaction networks between two linked residues suggested that several interactions between the PH domain and RhoA were observed to be capable of linking membrane interacting residues on the PH domain to many key residues in the RhoA switch region such as Thr-37. Residues such as Lys-104 of RhoA were found to propagate interactions from the PH domain all the way to the GDP binding site (Figure S7B), and have the potential to propagate allosteric interactions that could influence GEF

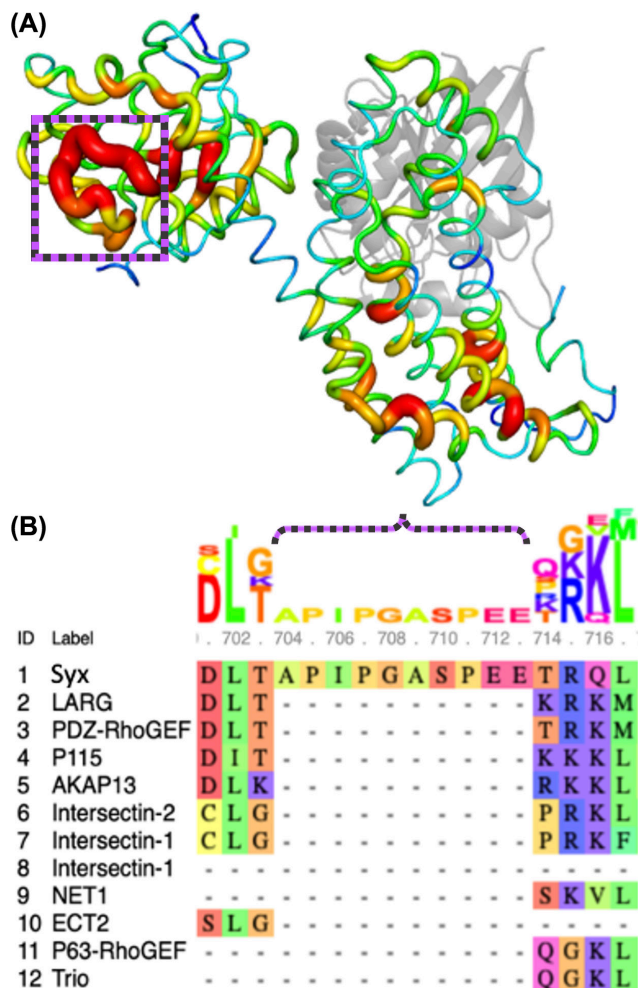


**FIGURE 5** The ratio of non-polar to polar residues that are solvent accessible, as scored by the protein-sol server. Thicker red regions have the highest ratio of non-polar residues, while thin blue patches have the lowest ratio of non-polar to polar residues. The purple-black dashed bracket and corresponding purple-black dashed box indicate the unique hydrophobic loop on the Syx PH domain in the multiple sequence alignment. The analysis reveals a large, membrane facing, non-polar loop on the PH domain which is not conserved in any other homologous RhoGEF structures.

activity when the GEF-RhoA complex is in the presence of a membrane.

Additionally, the modeled geranylgeranyl linked cysteine-190 at the C-terminus of RhoA was observed to make several transient interactions with the membrane embedded PH domain of Syx (Figure 7A).

## 4 | DISCUSSION

Here we use a combination of protein expression, purification, spectroscopic and modeling techniques to characterize Syx, a partially soluble Dbl RhoGEF protein. Successful expression and purification of Syx was pivotal

for all biophysical characterization performed. The exploratory expression of the wild type mouse Syx gene initially displayed low expression and degradation when expressed in *E. coli*. The fact that codon optimization alleviated the formation of degradation products suggests that initial expression difficulties were caused by bacterial ribosomes being unable to complete production of the protein because of stoichiometric restrictions due to the presence of rare or promiscuous codons in the mouse gene. It is also notable that all solved structures of RhoGEFs were fragments of the DH and PH domain, expressed with the help of fusion constructs of either MBP or GST.<sup>64–66</sup> We also observed that MBP fusion enabled high level expression and protein solubility dropped dramatically upon TEV cleavage, suggesting that solubility was a culprit of the expression issues with these proteins and that hydrophobic loops might be exposed on the protein surface.

Protocols for production of a monodispersed sample of native Syx protein remain elusive despite numerous exhaustive attempts at construct and buffer optimization, including pH modulation, addition of several detergents, chaotropes, kosmotropes, and charged amino acids (arginine and glutamic acid).<sup>57,67</sup> Buffer and purification optimization is ongoing with the goal of minimizing aggregation and achieving a polydispersity index (PDI) of <0.2 which is ideal for crystallographic studies.

Low solubility is a major limitation for crystallographic studies which work best with high concentrations of protein. TEV cleavage of the purified MBP fusion protein produced an increasingly turbid suspension at concentrations above 4mg/ml, indicating the formation of large aggregates in solution without the solubility enhancing effects of the fusion tag. This was further corroborated by size exclusion chromatography. We have shown CD experiments that support the hypothesis that this protein is not forming a misfolded aggregate (Figure 4) and is instead forming non-stoichiometric homo-oligomers. This is further supported by the fact that this protein complex shows RhoA binding activity by SEC (Figure 3A) and dot blot (Figure S8). This suggests that disruption of the protein-protein interactions that lead to the formation of the large non-stoichiometric homo-oligomer could result in a protein sample which is suitable for structural studies.<sup>68–70</sup>

This hypothesis of non-specific interaction is potentially explained by the results of the protein-sol analysis which shows that this protein contains highly hydrophobic loops which may drive interaction (Figure 5, dashed purple box). The analysis also revealed highly charged domains with a large positively charged patch on the DH domain and negative charged regions on the PH domain (Figure S6). These patches may stick to each other without the steric bulk and entropically driven stabilizing effects of disordered regions that are present in the native

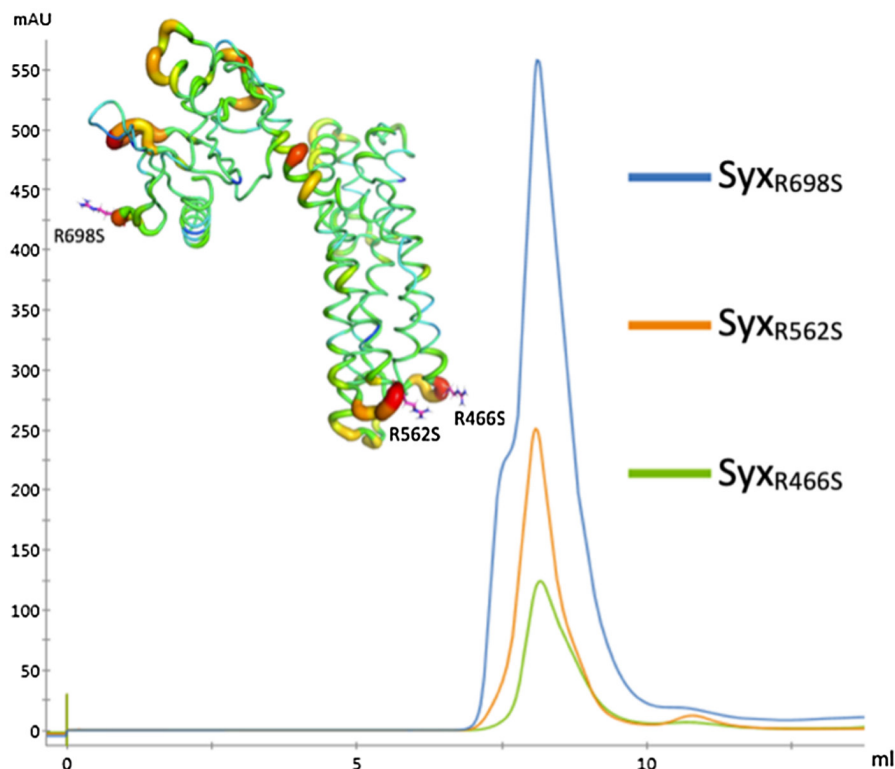


**FIGURE 6** Mutations to surface residues predicted by CamSol web server resulted in SEC peak shifts suggesting that these mutations produced improvements to problematic aggregation characteristics.

protein. Protein engineering efforts focused on removing the numerous highly exposed arginine residues and other surface facing residues known to cause nonspecific protein interactions such as methionine, tryptophan, tyrosine, and phenylalanine, presents a promising approach for producing monomeric protein suitable for structural studies that will be suitable for future drug design efforts.

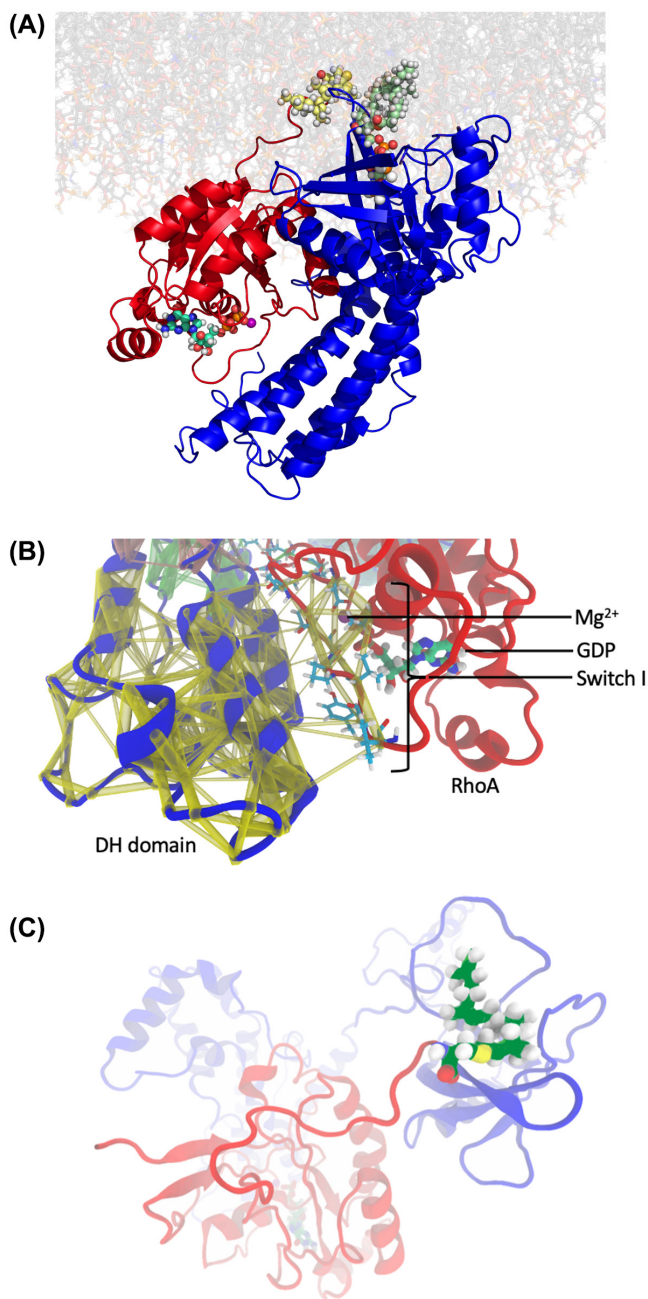
A complex structure of Syx bound to RhoA would be most useful for structurally guided drug design so optimized protocols for forming the complex while maintaining the integrity of the proteins is needed. RhoGEFs have highest affinity for apo RhoA so formation of apo RhoA is essential; however, RhoA has picomolar affinity for GDP.<sup>71</sup> The active site of RhoA contains a magnesium ion which forms multiple ionic interactions with the phosphate groups of GDP. Strategies to remove the tightly bound GDP require removal of the magnesium, either with excess EDTA, high concentrations of ammonium sulphate, aggressive buffer exchange, or the presence of an active GEF.

Ongoing work seeks to quantify Syx binding affinity to phosphoinositide lipids to characterize contextual protein localization in the cell and potentially establish if allosteric inhibition is possible. Syx is known to bind proteins associated with regulation of cell polarity and cell shape in the CRUMBS polarity complex, as well as stress fiber production and the maintenance of cell-cell junctions.<sup>4,72,73</sup>

In vivo, Syx is bound to the CRUMBS complex via the scaffold protein Mupp-1 and/or Patj.<sup>6,74,75</sup> Given the membrane trafficking at this site, it would make sense that the PH domain of this protein would likely bind PI(4,5)P2, the canonical ligand for PH domains,<sup>9,76</sup> because PI(4,5)P2 is also associated with actin cytoskeletal activity modulated by the CRUMBS polarity complex.<sup>77,78</sup> Active RhoA stimulates PIP 5-kinase and subsequent formation of PI(4,5)P2, implicating a positive feedback mechanism where active RhoA results in production of PI(4,5)P2, which recruits Syx to reactivate RhoA as part of a cell's polarity program.<sup>79,80</sup> Notably, at the leading edges of migrating endothelial cells Syx colocalizes with angiomin, another phosphoinositide binding protein with phosphorylation dependent oncogenic potential via the hippo pathway.<sup>21,81</sup> In the future, Large Unilamellar Vesicle (LUV) pull-down assays may answer these questions as well as guide ongoing purification and structural analysis strategies that include the addition of various lipids, membrane mimetics, and protein cofactors that may reduce unwanted interactions and ultimately allow for further characterization.

To our knowledge, all atom molecular dynamics simulations have never been performed on a RhoA-Dbl homology GEF complex on a membrane. These simulations revealed a network of interactions that facilitate GEF activity when bound to RhoA. The analysis revealed several interactions between RhoA and the PH domain, mediated





by hydrogen bonding networks between positively charged residues and PI(4,5)P<sub>2</sub> phospho-inositide headgroups (Figure S7A) which may represent a novel mechanism for allostery. This interaction may directly influence the active site of RhoA, as optimal path analysis of the dynamic network showed interactions at the membrane interface of the PH domain share covariance networks that form a link to the active site of RhoA via an optimal path traveling through a lipid headgroup (Figure 7B).

Even more intriguingly, simulations revealed novel interactions between the geranylgeranyl prenyl group ligated to the N-term of RhoA residue 191. These simulated interactions represent a hypothesis for a novel function of the PH domain in membrane associated GEFs. It is

conceivable that the PH domain constitutes a lipid binding site situated within the membrane that forms intermolecular interactions with the geranylgeranyl group and helps position RhoA for efficient guanine exchange and alter the binding mode between the DH and PH domains in such a way that it could impinge on the switch regions of RhoA, and help facilitate the opening of the binding site, thus enhancing the release of GDP (Figure S7A). These C-terminal residues and post-translational modifications of RhoA are missing from all current GEF-RhoA complex structures. Given that the addition of liposomes to activity assays has been shown to enhance activity in other related systems, it is conceivable that this type of interaction is contributing to guanine exchange catalysis. Structural and kinetic studies with GEFs bound to geranylgeranylated RhoA in the presence of a membrane are required to confirm this hypothesis which may be the subject of future work.

Subsequent attempts at generating monodispersed Syx will be made by co-expressing Syx with RhoA in insect cells, as well as purification strategies that take into account the amphiphilic nature of this membrane-associated protein. The modeling efforts included in this paper have provided insights for ongoing future work including mutagenesis efforts to engineer the surface of Syx to replace residues that are likely to contribute to nonspecific protein interactions as well as several provocative insights into the potential effect of membranes on the structure and function of this protein that may support establishment of new druggable sites with further experimental validation.

Subsequent attempts at generating monodispersed Syx will be made by co-expressing Syx with RhoA in insect cells, as well as purification strategies that take into account the amphiphilic nature of this membrane-associated protein. The modeling efforts included in this paper have provided insights for ongoing future work including mutagenesis efforts to engineer the surface of Syx to replace residues that are likely to contribute to nonspecific protein interactions as well as several provocative insights into the potential effect of membranes on the structure and function of this protein that may support establishment of new druggable sites with further experimental validation.

#### AUTHOR CONTRIBUTIONS

Ryan J. Boyd, Tien L. Olson, James D. Zook, Debra T. Hansen, and Petra Fromme designed and planned research, Ryan J. Boyd, Tien L. Olson, James D. Zook, Debra T. Hansen, and Petra Fromme analyzed and

interpreted data, Ryan J. Boyd, Manuel Aceves, and Derek Stein performed research, Debra T. Hansen, Felicia M. Craciunescu, Panos Z. Anastasiadis, Wan-Hsin Lin, Abhishek Singharoy, and Petra Fromme contributed reagents and resources, Ryan J. Boyd, Tien L. Olson, Debra T. Hansen, and Petra Fromme wrote and edited the paper with comments and edits from all authors.

## ACKNOWLEDGEMENTS

This work was supported by Mayo-ASU Structural Biology Alliance funded by Mayo Clinic and the Biodesign Center for Applied Structural Discovery at Arizona State University, and by NIH R01NS101721-A1 to PZA. We thank Alex Baker, Daniel Ari Friedman, Megumi Ashley Satkowski, Nattö Satkowski, and John Vant for editing assistance.

## DISCLOSURES

Authors declare no known conflicts of interests.

## DATA AVAILABILITY STATEMENT

All data supporting the findings of this study are available in the methods and supplemental material. Molecular dynamics simulation trajectory and parameter files and protein model files are available from the authors upon request.

## ORCID

Ryan J. Boyd  <https://orcid.org/0000-0002-6704-8696>

Petra Fromme  <https://orcid.org/0000-0003-0953-4909>

## REFERENCES

- Ostrem JM, Peters U, Sos ML, Wells JA, Shokat KM. K-Ras(G12C) inhibitors allosterically control GTP affinity and effector interactions. *Nature*. 2013;503:548-551.
- Fort P, Blangy A. The evolutionary landscape of Dbl-like RhoGEF families: adapting eukaryotic cells to environmental signals. *Genome Biol Evol*. 2017;9:1471-1486.
- Snyder JT, Worthylake DK, Rossman KL, et al. Structural basis for the selective activation of Rho GTPases by Dbl exchange factors. *Nat Struct Biol*. 2002;9:468-475.
- Sahai E, Marshall CJ. ROCK and Dia have opposing effects on adherens junctions downstream of Rho. *Nat Cell Biol*. 2002;4:408-415.
- Cherfils J, Zeghouf M. Regulation of small GTPases by GEFs, GAPs, and GDIs. *Physiol Rev*. 2013;93:269-309.
- Ngok SP, Geyer R, Liu M, et al. VEGF and Angiopoietin-1 exert opposing effects on cell junctions by regulating the Rho GEF Syx. *J Cell Biol*. 2012;199:1103-1115.
- Ngok SP, Geyer R, Kourtidis A, Storz P, Anastasiadis PZ. Phosphorylation-mediated 14-3-3 protein binding regulates the function of the rho-specific guanine nucleotide exchange factor (RhoGEF) Syx. *J Biol Chem*. 2013;288:6640-6650.
- Jaiswal M, Dvorsky R, Ahmadian MR. Deciphering the molecular and functional basis of Dbl family proteins: a novel systematic approach toward classification of selective activation of the Rho family proteins. *J Biol Chem*. 2013;288:4486-4500.
- Harlan JE, Yoon HS, Hajduk PJ, Fesik SW. Structural characterization of the interaction between a pleckstrin homology domain and phosphatidylinositol 4,5-bisphosphate. *Biochemistry*. 1995;34:9859-9864.
- Harlan JE, Hajduk PJ, Yoon HS, Fesik SW. Pleckstrin homology domains bind to phosphatidylinositol-4,5-bisphosphate. *Nature*. 1994;371:168-170.
- Chen Z, Guo L, Sprang SR, Sternweis PC. Modulation of a GEF switch: autoinhibition of the intrinsic guanine nucleotide exchange activity of p115-RhoGEF. *Protein Sci*. 2011;20:107-117.
- Roy NS, Yohe ME, Randazzo PA, Gruschus JM. Allosteric properties of PH domains in Arf regulatory proteins. *Cell Logist*. 2016;6:e1181700.
- Jian X, Gruschus JM, Sztul E, Randazzo PA. The pleckstrin homology (PH) domain of the Arf exchange factor Brag2 is an allosteric binding site. *J Biol Chem*. 2012;287:24273-24283.
- Bielnicki JA, Shkumatov AV, Derewenda U, Somlyo AV, Svergun DI, Derewenda ZS. Insights into the molecular activation mechanism of the RhoA-specific guanine nucleotide exchange factor, PDZRhoGEF. *J Biol Chem*. 2011;286:35163-35175.
- Zheng M, Cierpicki T, Momotani K, et al. On the mechanism of autoinhibition of the RhoA-specific nucleotide exchange factor PDZRhoGEF. *BMC Struct Biol*. 2009;9:36.
- Viaud J, Gaits-Iacovoni F, Payrastré B. Regulation of the DH-PH tandem of guanine nucleotide exchange factor for Rho GTPases by phosphoinositides. *Adv Biol Regul*. 2012;52:303-314.
- Vigil D, Cherfils J, Rossman KL, Der CJ. Ras superfamily GEFs and GAPs: validated and tractable targets for cancer therapy? *Nat Rev Cancer*. 2010;10:842-857.
- Aspenström P. Activated Rho GTPases in cancer—the beginning of a new paradigm. *Int J Mol Sci*. 2018;19:3949.
- Dachsel JC, Ngok SP, Lewis-Tuffin LJ, et al. The Rho guanine nucleotide exchange factor Syx regulates the balance of dia and ROCK activities to promote polarized-cancer-cell migration. *Mol Cell Biol*. 2013;33:4909-4918.
- Qian M, Chen Z, Wang S, et al. PLEKHG5 is a novel prognostic biomarker in glioma patients. *Int J Clin Oncol*. 2019;24:1350-1358.
- Ernkvist M, Luna Persson N, Audebert S, et al. The Amot/Patj/Syx signaling complex spatially controls RhoA GTPase activity in migrating endothelial cells. *Blood*. 2009;113:244-253.
- Garnaas MK, Moodie KL, Liu ML, et al. Syx, a RhoA guanine exchange factor, is essential for angiogenesis in vivo. *Circ Res*. 2008;103:710-716.
- Jubb H, Higuero AP, Winter A, Blundell TL. Structural biology and drug discovery for protein-protein interactions. *Trends Pharmacol Sci*. 2012;33:241-248.
- Luningschror P, Binotti B, Dombert B, et al. Plekhg5-regulated autophagy of synaptic vesicles reveals a pathogenic mechanism in motoneuron disease. *Nat Commun*. 2017;8:678.
- Structural Genomics, C., China Structural Genomics, C., Northeast Structural Genomics, C., et al. Protein production and purification. *Nat Methods*. 2008;5:135-146.
- Yang J, Yan R, Roy A, Xu D, Poisson J, Zhang Y. The I-TASSER Suite: protein structure and function prediction. *Nat Methods*. 2015;12:7-8.

27. Buchan DWA, Jones DT. The PSIPRED protein analysis workbench: 20 years on. *Nucleic Acids Res.* 2019;47:W402-W407.
28. Goldschmidt L, Cooper DR, Derewenda ZS, Eisenberg D. Toward rational protein crystallization: a Web server for the design of crystallizable protein variants. *Protein Sci.* 2007;16:1569-1576.
29. Slabinski L, Jaroszewski L, Rychlewski L, Wilson IA, Lesley SA, Godzik A. XtalPred: a web server for prediction of protein crystallizability. *Bioinformatics.* 2007;23:3403-3405.
30. Katoh K, Rozewicki J, Yamada KD. MAFFT online service: multiple sequence alignment, interactive sequence choice and visualization. *Brief Bioinform.* 2019;20:1160-1166.
31. Combs SA, Deluca SL, Deluca SH, et al. Small-molecule ligand docking into comparative models with Rosetta. *Nat Protoc.* 2013;8:1277-1298.
32. Lyskov S, Gray JJ. The RosettaDock server for local protein-protein docking. *Nucleic Acids Res.* 2008;36:W233-W238.
33. Yamamoto E, Kalli AC, Yasuoka K, Sansom MSP. Interactions of pleckstrin homology domains with membranes: adding back the bilayer via high-throughput molecular dynamics. *Structure.* 2016;24:1421-1431.
34. Naughton FB, Kalli AC, Sansom MSP. Modes of interaction of pleckstrin homology domains with membranes: toward a computational biochemistry of membrane recognition. *J Mol Biol.* 2018;430:372-388.
35. Yamamoto E. Computational and theoretical approaches for studies of a lipid recognition protein on biological membranes. *Biophys Physicobiol.* 2017;14:153-160.
36. DeLuca S, Khar K, Meiler J. Fully flexible docking of medium sized ligand libraries with RosettaLigand. *PLoS One.* 2015;10:e0132508.
37. Kothiwale S, Mendenhall JL, Meiler J. BCL::Conf: small molecule conformational sampling using a knowledge based rotamer library. *J Cheminform.* 2015;7:47.
38. Lomize MA, Pogozheva ID, Joo H, Mosberg HI, Lomize AL. OPM database and PPM web server: resources for positioning of proteins in membranes. *Nucleic Acids Res.* 2012;40:D370-D376.
39. Wu EL, Cheng X, Jo S, et al. CHARMM-GUI Membrane Builder toward realistic biological membrane simulations. *J Comput Chem.* 2014;35:1997-2004.
40. Lee J, Cheng X, Swails JM, et al. CHARMM-GUI input generator for NAMD, GROMACS, AMBER, OpenMM, and CHARMM/OpenMM simulations using the CHARMM36 additive force field. *J Chem Theory Comput.* 2016;12:405-413.
41. Kim S, Lee J, Jo S, Brooks CL 3rd, Lee HS, Im W. CHARMM-GUI ligand reader and modeler for CHARMM force field generation of small molecules. *J Comput Chem.* 2017;38:1879-1886.
42. Phillips JC, Braun R, Wang W, et al. Scalable molecular dynamics with NAMD. *J Comput Chem.* 2005;26:1781-1802.
43. Huang J, Rauscher S, Nawrocki G, et al. CHARMM36m: an improved force field for folded and intrinsically disordered proteins. *Nat Methods.* 2017;14:71-73.
44. Humphrey W, Dalke A, Schulten K. VMD: visual molecular dynamics. *J Mol Graph.* 1996;14(33-38):27-38.
45. Sethi A, Eargle J, Black AA, Luthey-Schulten Z. Dynamical networks in tRNA:protein complexes. *Proc Natl Acad Sci USA.* 2009;106:6620-6625.
46. Sormanni P, Aprile FA, Vendruscolo M. The CamSol method of rational design of protein mutants with enhanced solubility. *J Mol Biol.* 2015;427:478-490.
47. Liu Y, Kuhlman B. RosettaDesign server for protein design. *Nucleic Acids Res.* 2006;34:W235-W238.
48. Robertson KE, Truong CD, Craciunescu FM, et al. Membrane directed expression in Escherichia coli of BBA57 and other virulence factors from the Lyme disease agent Borrelia burgdorferi. *Sci Rep.* 2019;9:17606.
49. Mazhab-Jafari MT, Marshall CB, Smith M, et al. Real-time NMR study of three small GTPases reveals that fluorescent 2'(3')-O-(N-methylanthraniloyl)-tagged nucleotides alter hydrolysis and exchange kinetics. *J Biol Chem.* 2010;285:5132-5136.
50. Greenfield NJ. Using circular dichroism spectra to estimate protein secondary structure. *Nat Protoc.* 2006;1:2876-2890.
51. Micsonai A, Wien F, Kernya L, et al. Accurate secondary structure prediction and fold recognition for circular dichroism spectroscopy. *Proc Natl Acad Sci USA.* 2015;112:E3095-E3103.
52. Perez-Iratxeta C, Andrade-Navarro MA. K2D2: estimation of protein secondary structure from circular dichroism spectra. *BMC Struct Biol.* 2008;8:25.
53. Miles AJ, Ramalli SG, Wallace BA. DichroWeb, a website for calculating protein secondary structure from circular dichroism spectroscopic data. *Protein Sci.* 2021;31:37-46.
54. Mavridis L, Janes RW. PDB2CD: a web-based application for the generation of circular dichroism spectra from protein atomic coordinates. *Bioinformatics.* 2017;33:56-63.
55. Yang J, Zhang Y. Protein structure and function prediction using I-TASSER. *Curr Protoc Bioinf.* 2015;52:5.8.1-5.8.15.
56. Jones DT, Cozzetto D. DISOPRED3: precise disordered region predictions with annotated protein-binding activity. *Bioinformatics.* 2015;31:857-863.
57. Lebediker M, Danieli T. Production of prone-to-aggregate proteins. *FEBS Lett.* 2014;588:236-246.
58. Ranjbar B, Gill P. Circular dichroism techniques: biomolecular and nanostructural analyses—a review. *Chem Biol Drug Des.* 2009;74:101-120.
59. Hebditch M, Warwicker J. Web-based display of protein surface and pH-dependent properties for assessing the developability of biotherapeutics. *Sci Rep.* 2019;9:1969.
60. Chan P, Curtis RA, Warwicker J. Soluble expression of proteins correlates with a lack of positively-charged surface. *Sci Rep.* 2013;3:3333.
61. Abdul Azeez KR, Knapp S, Fernandes JM, Klussmann E, Elkins JM. The crystal structure of the RhoA-AKAP-Lbc DH-PH domain complex. *Biochem J.* 2014;464:231-239.
62. Vetter IR, Wittinghofer A. The guanine nucleotide-binding switch in three dimensions. *Science.* 2001;294:1299-1304.
63. Rossman KL, Sondek J. Larger than Dbl: new structural insights into RhoA activation. *Trends Biochem Sci.* 2005;30:163-165.
64. Kosobokova EN, Skrypnik KA, Kosorukov VS. Overview of fusion tags for recombinant proteins. *Biochemistry (Mosc).* 2016;81:187-200.
65. Pina AS, Lowe CR, Roque AC. Challenges and opportunities in the purification of recombinant tagged proteins. *Biotechnol Adv.* 2014;32:366-381.
66. Esposito D, Chatterjee DK. Enhancement of soluble protein expression through the use of fusion tags. *Curr Opin Biotechnol.* 2006;17:353-358.
67. Bondos SE, Bicknell A. Detection and prevention of protein aggregation before, during, and after purification. *Anal Biochem.* 2003;316:223-231.



68. Chikumi H, Barac A, Behbahani B, et al. Homo- and hetero-oligomerization of PDZ-RhoGEF, LARG and p115RhoGEF by their C-terminal region regulates their in vivo Rho GEF activity and transforming potential. *Oncogene*. 2004;23:233-240.
69. Austerberry JI, Thistlethwaite A, Fisher K, et al. Arginine to lysine mutations increase the aggregation stability of a single-chain variable fragment through unfolded-state interactions. *Biochemistry*. 2019;58:3413-3421.
70. Garrard SM, Longenecker KL, Lewis ME, Sheffield PJ, Derewenda ZS. Expression, purification, and crystallization of the RGS-like domain from the Rho nucleotide exchange factor, PDZ-RhoGEF, using the surface entropy reduction approach. *Protein Expr Purif*. 2001;21:412-416.
71. Zhang B, Zhang Y, Wang Z, Zheng Y. The role of Mg<sup>2+</sup> cofactor in the guanine nucleotide exchange and GTP hydrolysis reactions of Rho family GTP-binding proteins. *J Biol Chem*. 2000;275:25299-25307.
72. Ngok SP, Lin WH, Anastasiadis PZ. Establishment of epithelial polarity—GEF who's minding the GAP? *J Cell Sci*. 2014;127:3205-3215.
73. Hanna S, El-Sibai M. Signaling networks of Rho GTPases in cell motility. *Cell Signal*. 2013;25:1955-1961.
74. Ngok SP, Anastasiadis PZ. Rho GEFs in endothelial junctions: effector selectivity and signaling integration determine junctional response. *Tissue Barriers*. 2013;1:e27132.
75. Wu C, Agrawal S, Vasanji A, et al. Rab13-dependent trafficking of RhoA is required for directional migration and angiogenesis. *J Biol Chem*. 2011;286:23511-23520.
76. Cozier GE, Carlton J, Bouyoucef D, Cullen PJ. Membrane targeting by pleckstrin homology domains. *Curr Top Microbiol Immunol*. 2004;282:49-88.
77. Pilot F, Philippe JM, Lemmers C, Lecuit T. Spatial control of actin organization at adherens junctions by a synaptotagmin-like protein. *Nature*. 2006;442:580-584.
78. Lattner J, Leng W, Knust E, Brankatschk M, Flores-Benitez D. Crumbs organizes the transport machinery by regulating apical levels of PI(4,5)P2 in Drosophila. *Elife*. 2019;8:e50900.
79. Chong LD, Traynor-Kaplan A, Bokoch GM, Schwartz MA. The small GTP-binding protein Rho regulates a phosphatidylinositol 4-phosphate 5-kinase in mammalian cells. *Cell*. 1994;79:507-513.
80. Nelson WJ. Remodeling epithelial cell organization: transitions between front-rear and apical-basal polarity. *Cold Spring Harb Perspect Biol*. 2009;1:a000513.
81. Chan SW, Lim CJ, Chong YF, Pobbati AV, Huang C, Hong W. Hippo pathway-independent restriction of TAZ and YAP by angiomin. *J Biol Chem*. 2011;286:7018-7026.

## SUPPORTING INFORMATION

Additional supporting information may be found in the online version of the article at the publisher's website.

**How to cite this article:** Boyd RJ, Olson TL, Zook JD, et al. Characterization and computational simulation of human Syx, a RhoGEF implicated in glioblastoma. *FASEB J*. 2022;36:e22378. doi:[10.1096/fj.202101808RR](https://doi.org/10.1096/fj.202101808RR)